Cooperative Gas Adsorption without a Phase Transition in Metal-Organic Frameworks

Joyjit Kundu,[1,2,*] Jürgen F. Stilck,[3] Jung-Hoon Lee,[1,4] Jeffrey B. Neaton,[1,4,5] David Prendergast,[1,†] and Stephen Whitelam[1,‡]

[1]*Molecular Foundry, Lawrence Berkeley National Laboratory, Berkeley, California 94720, USA*
[2]*Department of Chemistry, Duke University, Durham, North Carolina 27708, USA*
[3]*Instituto de Física and National Institute of Science and Technology for Complex Systems, Universidade Federal Fluminense, Avenida Litorânea s/n, 24210-346—Niterói, RJ, Brazil*
[4]*Department of Physics, University of California, Berkeley, California 94720-7300, USA*
[5]*Kavli Energy Nanosciences Institute at Berkeley, Berkeley, California 94720, USA*

(Received 12 December 2017; published 3 July 2018)

Cooperative adsorption of gases by porous frameworks, which permits more efficient uptake and removal than the more usual noncooperative (Langmuir-type) adsorption, usually results from a phase transition of the framework. Here we show how cooperativity emerges in the class of metal-organic frameworks mmen-M_2(dobpdc) in the absence of a phase transition. Our study provides a microscopic understanding of the emergent features of cooperative binding, including the position, slope, and height of the isotherm step, and indicates how to optimize gas storage and separation in these materials.

Introduction.—Metal-organic frameworks (MOFs), porous crystalline materials with tunable molecular properties and large internal surface areas, are promising candidates for gas capture and separation [1–6]. In equilibrium [7], most gas adsorption within MOFs can be described by Langmuir-type adsorption isotherms, in which the quantity of adsorbed gas varies gradually with pressure or temperature [3,10–14]. It is technologically more convenient, however, to have the quantity of adsorbed gas vary in an abrupt way with pressure and temperature. This phenomenon is known as cooperative adsorption and is exhibited by a small handful of gas-framework combinations. These include CO adsorption in Fe_2Cl_2(bbta) [15], CH_4 adsorption in Fe(bdp) [16], and CO_2 adsorption in diamine-appended MOFs [17,18]; in MIL-53 [19,20]; and in a bifunctional MOF [21]. Cooperativity in most of these cases is attributed to a first-order phase transition [22–27] or a dynamic rearrangement [22,28] of the framework. However, for the case of diamine-appended MOFs [mmen-, en-, men-, or den-M_2(dobpdc), where M stands for the metal Mg, Mn, Fe, Co, or Zn], there exists no evidence of structural dynamism or a phase transition of the structure or adsorbate—which forms one-dimensional ammonium carbamate chains at high pressure—making the origin of cooperativity unclear.

Here we show how this cooperativity emerges in the absence of an underlying phase transition. Experimental studies and quantum mechanical density-functional theory (DFT) calculations had previously revealed that, at a low partial pressure of CO_2, the gas molecules are adsorbed as single molecules or as carbamic acid pairs [29]. At a high partial pressure, by contrast, CO_2 undergoes chemisorption, by forming one-dimensional ammonium carbamate

chains that run down the channels of the MOF, along the c axis [17]. The statistical mechanics of one-dimensional structures [30] indicates that chain formation cannot be accompanied by a phase transition: Finite-temperature phase transitions in one dimension require long-range interactions, and there are no indications of long-range interactions in the system (either direct or mediated by the framework). By mapping CO_2 adsorption in mmen-M_2(dobpdc) to an exactly solvable statistical mechanical model, parameterized by our DFT calculations, we show that the mean chain length of CO_2 within the MOF pores undergoes a sharp but finite change with pressure, leading to cooperativity in the absence of an underlying phase transition. Amine-functionalized MOFs have emerged as one of the best framework types for CO_2 capture and separation, because, unusually for MOFs, they capture CO_2 selectively in the presence of water [17,18,31]. Our results provide a microscopic understanding of cooperativity in these MOFs and reveal strategies for its control. In what follows, we describe our calculations and their implication for optimizing CO_2 capture in experiments.

Model.—We start by considering binding geometries and affinities of CO_2 within mmen-M_2(dobpdc). CO_2 can bind within this class of MOFs as (i) a single molecule, (ii) a bound (carbamic acid) pair, or (iii) as part of a polymerized (ammonium carbamate) chain of molecules involving the ligands through its insertion at the metal sites [17]. Pairs form in the *ab* plane [29]; see Figs. 1(a) and 1(b). By contrast, chains are formed parallel to the c axis, along any of six lanes around the periphery of the MOF channel, but usually do not interact in the *ab* plane [32]. For mmen-MOF built from the metals Mg, Mn, Fe, Co, and Zn, experiments and DFT calculations show that molecules in
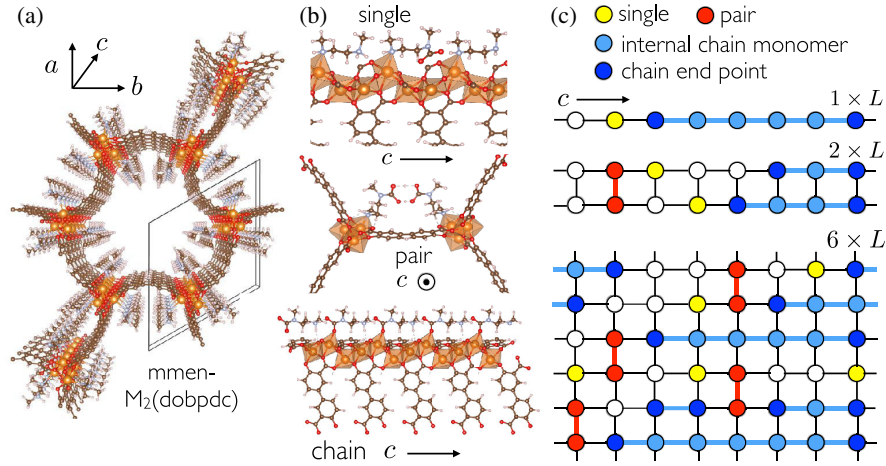
FIG. 1. (a) Hexagonal channel of mmen-M_2(dobdpc) (where M stands for the metal Mg, Mn, Fe, Co, Zn, or Ni). (b) The three possible conformations of adsorbed CO_2 within this class of MOF. (c) Our statistical mechanical models of mmen-M_2(dobdpc), in example configurations.

the chain conformation are lower in energy than molecules in the single and pair conformations [17,29] (see Table SI in Supplemental Material [33]). Our DFT calculations (see Supplemental Material [33], Secs. S1 and S2) also indicate that CO_2 molecules at the end of a chain are higher in energy than those in the interior of a chain. Entropically, by contrast, the chain conformation is less favorable than the other two conformations.

The thermodynamics of this system can be described by the equilibrium polymerization model [34], sketched in Fig. 1(c). This is a lattice model, extended in one dimension (corresponding to the c axis of the MOF). Lattice sites can be vacant, occupied by a single particle (a CO_2 molecule), or occupied by a particle that is a member of a pair or a chain of particles. We further distinguish chain end sites from chain interior sites. In some versions of mmen-M_2 (dobdpc), e.g., where M is Mg or Mn, the bound-pair binding affinity is small enough, relative to the chain, that it can be ignored [29] (see Table SI in Supplemental Material [33]). In these cases, it is sufficient to consider a one-lane model, which represents one of the six lanes running along the c axis. In the presence of the bound-pair conformation, we need to allow a finite extent in the ab direction. A six-lane model is then required to describe all possible CO_2 conformations within the six-lane MOF channel. We have also considered a two-lane model, because the distance between the lanes in some versions of mmen-M_2(dobdpc) is such that the framework is best described as three independent two-lane structures (i.e., CO_2 pairs can bridge only alternate pairs of lanes). We have solved the one-, two-, and six-lane models exactly. The one-lane model captures the basic physics of cooperative binding in all experiments we consider. The two-lane and six-lane models capture, in addition, fine features of adsorption isotherms seen in MOFs in which pair binding is significant (see Supplemental Material [33], Sec. S4, for details).

Model solution.—We start with the one-lane model. Let the statistical weights for a single bound molecule, a molecule internal to a chain, and a molecule at either end point of a chain be $g_1 W_1$, $g_{\text{int}} W_{\text{int}}$, and $g_{\text{end}} W_{\text{end}}$, respectively. Here $g_\alpha = V_\alpha \Lambda^{-3} q_{\text{inter},\alpha}$ ($\alpha = \{1, \text{int}, \text{end}\}$). The factor $V_\alpha \Lambda^{-3}$ arises from the configurational partition sum and is related to the translational entropy of the adsorbate; Λ is the de Broglie wavelength; and V_α is the free volume accessible to the adsorbate in the conformation α [22]. The factor $q_{\text{inter},\alpha}$ is the partition sum of CO_2 due to its internal degrees of freedom in the conformation α [35]. These statistical weights can be related to the energy of a particle in conformation α via $W_\alpha = \exp[\beta(\mu - E_\alpha)]$, where $\beta \equiv 1/(k_B T)$ and μ is the chemical potential, set by the pressure P of CO_2 in the bulk. We convert μ to P using the ideal gas relation for a linear triatomic molecule, $e^{\beta\mu} = \beta P \Lambda^3 / q_{\text{inter,bulk}}$ [36]. To simplify notation, we define $K_\alpha \equiv g_\alpha W_\alpha$. We then have $K_\alpha \approx \beta P V_\alpha e^{-\beta E_\alpha}$ [37]. We set $V_1 = 500$ Å^3, $V_{\text{int}} = V_{\text{end}} = 11$ Å^3 using simple geometric arguments (see Supplemental Material [33], Sec. S5): The single bound CO_2 molecule has orientational entropy associated with the corresponding diamine, while CO_2 in the chain conformation is almost frozen.

We solve this model in the thermodynamic limit, using standard transfer-matrix methods [34], to give the free energy $f = -k_B T \ln \lambda_+$ (λ_+ is the largest eigenvalue of the transfer matrix—see Supplemental Material [33], Sec. S3, for details), where

$$2\lambda_+ = 1 + K_1 + K_{\text{int}} + \sqrt{(1 + K_1 - K_{\text{int}})^2 + 4K_{\text{end}}^2}. \quad (1)$$

The free energy has a singularity (and so admits a phase transition) only in the experimentally inaccessible limit in which chain end points are energetically infinitely unfavorable ($K_{\text{end}} = 0$, with $1 + K_1 = K_{\text{int}}$). For experimental
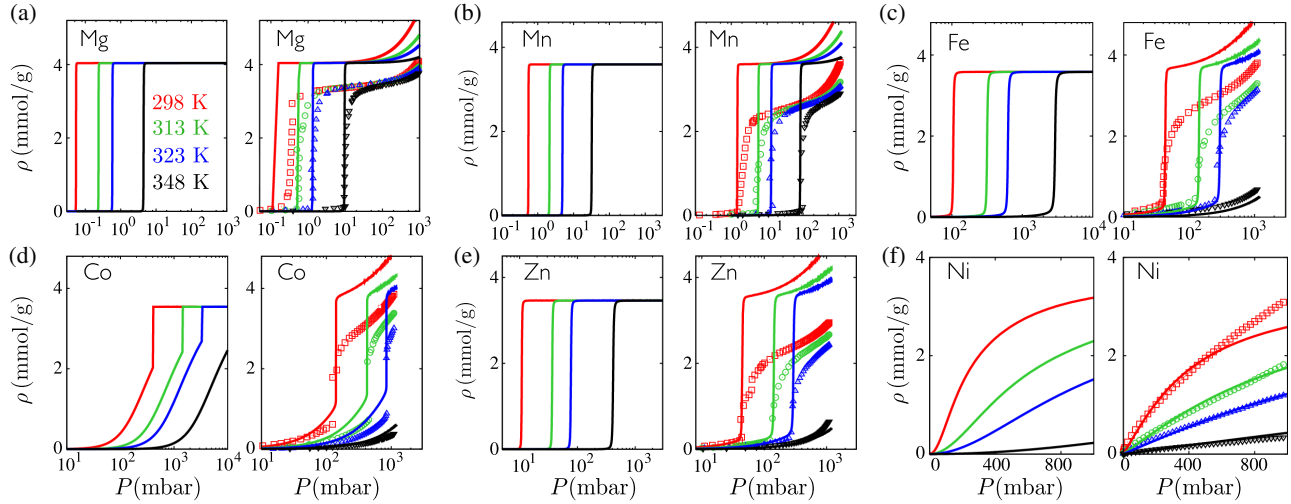
FIG. 2. Isotherms calculated from our model of mmen-M_2(dobpdc) (lines) versus experimental data (symbols). In the left-hand panels the model is parameterized using quantum mechanical data; it predicts the existence of the sharp isotherms, and the trend of step pressure with temperature, seen in experiments [17]. In the right-hand panels, we use the experimental binding enthalpy values, where available, to identify the model parameter V_{int} that gives the best match with experimental data; see Table SII [33] [for Ni, we vary the parameter E_d to obtain the best fit (see Supplemental Material [33], Sec. S6), and consider secondary binding sites and a different mode of monomer binding]. For Mg and Mn, we ignore the pair conformation, which is energetically disfavored, and use the one-lane model. The other panels are derived from the six-lane model, which accounts for pair binding. Here the model parameters E_1, E_d, and E_{int} are taken from Table SI in Supplemental Material [33]; $V_1 = 500$ Å and $V_d = 75$ Å.

parameters, the free energy is analytic; thus, no phase transition occurs.

Model-experiment comparison.—Despite the absence of a phase transition, the isotherm of adsorbed CO_2 versus pressure displays a sharp step (when $K_{int} > K_{end}, K_1$) similar to those seen in experiments; see Fig. 2. To convert lattice-site occupancies $\rho = -\beta P(\partial f/\partial P)$ to experimental units, we multiply our calculated density by the theoretical maximum uptake capacity (q_M) of the MOF for each M. The values of q_M are listed in Table SIII in Supplemental Material [33]. For each metal, the isotherms in the left-hand panels in Fig. 2 are generated by using the model in "predictive" mode, with binding energy parameters taken from DFT calculations (Table SI in Supplemental Material [33]). In the right-hand panels, we use binding-energy inputs taken from experiments. The comparison shows that a combination of quantum and statistical mechanics, with no experimental input, can reproduce the sharp step seen in experimental isotherms and can capture the trend in the step pressure with the temperature.

For the metals Mg and Mn, considered in Figs. 2(a) and 2(b), we use the one-lane model, because pair binding is energetically disfavored. For the other metals, we use the six-lane model (detailed in Supplemental Material [33], Sec. S4), because the bound-pair conformation, characterized by binding energy E_d and free volume V_d, is free-energetically significant (Table SI in Supplemental Material [33]). For Co, the rise of the isotherm before the step results from a proliferation of CO_2 pairs (due to a higher statistical weight) at low pressures. For nickel, the chain

conformation is not statistically favorable even at high pressures (Table SI in Supplemental Material [33]); thus, chain polymerization does not occur in the pressure range shown, explaining the absence of a step in the isotherms [Fig. 2(f)].

The basic physics of adsorption in all cases is captured by the simple considerations described above. The step position is very sensitive to the statistical weight of the chain conformation. Small uncertainties in binding energies (calculated via DFT) and the free volume parameters (estimated geometrically) can alter the step position significantly, and both types of uncertainty contribute to the quantitative differences between the step position measured experimentally and obtained by the model in predictive mode (see Fig. S1 [33]). In the right-hand panels in Fig. 2, we show that additional fine features of binding, such as the rise of isotherms before and after the step, can be captured by including within the model two additional physical ingredients, namely, the existence of secondary binding sites and of a different mode of monomer binding. Details of these calculations are given in Supplemental Material [33], Sec. S6. Thus, the model can provide insight into both the basic physics and the fine details of cooperative binding (e.g., the occupancy of different species as a function of pressure, measurable in NMR experiments; see Fig. S2 [33]).

Origin of cooperative binding.—The microscopic origin of the step in adsorption isotherms is a sudden but finite increase, with pressure, of the mean length of chains of CO_2. The fraction of chains of length ℓ, r_ℓ, can be
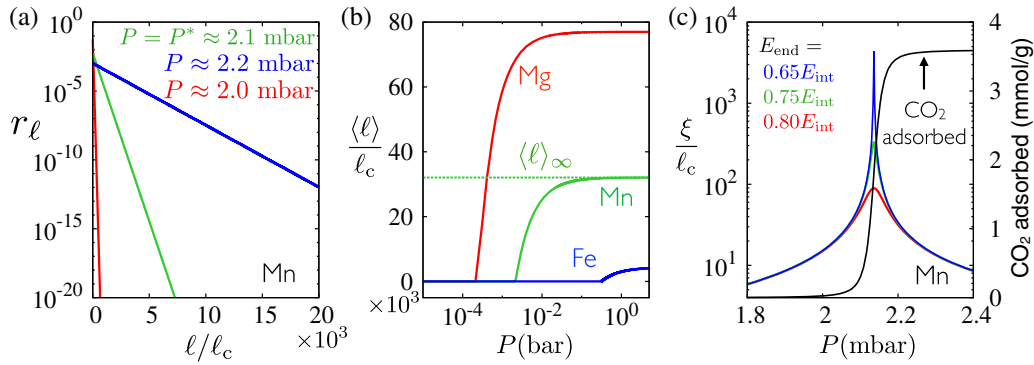
FIG. 3. (a) Chain-length distribution r_ℓ at different pressures for Mn at 313 K. (b) Mean chain length $\langle \ell \rangle$ as a function of pressure for different metals at 313 K. Here the length is expressed in units of $\ell_c \equiv 7$ Å, the unit-cell spacing of the crystal structure along the c axis. (c) Bond-bond correlation length ξ (in units of c spacing) as a function of pressure P for Mn at 313 K (colored lines), together with the adoption isotherm. Note that ξ grows exponentially with the energy cost for chain termini, E_{end}, for a given internal chain-monomer energy E_{int}.

expressed in terms of densities of chain-internal monomers (ρ_{int}) and end points (ρ_{end}), as

$$r_\ell = \frac{\rho_{end}}{\rho_{end} + 2\rho_{int}} \exp[-(\ell - 2)/\ell_0], \qquad (2)$$

where $\ell_0 \equiv -1/\ln[2\rho_{int}/(\rho_{end} + 2\rho_{int})]$; $\rho_{end} = 2K_{end}^2 \times \omega(1 - \omega K_{int})/D$; $\rho_{int} = K_{end}^2 \omega(\omega K_{int})/D$; $D = (1 + K_1) \times (1 - \omega K_{int})^2 + K_{end}^2 \omega(2 - \omega K_{int})$; and $\omega \equiv 1/\lambda_+$ (Ref. [38] and Supplemental Material [33], Sec. S7). The average chain length is $\langle \ell \rangle = 2 + \rho_{end}\ell_0^2/(\rho_{end} + 2\rho_{int})$.

The chain-length distribution for the one-lane model, Eq. (2), decays exponentially at all pressures, including at the step pressure P^* (which satisfies $d^2\rho/dP^2|_{P^*} = 0$). In Fig. 3(a), we plot r_ℓ for Mn. In Fig. 3(b), we plot the mean chain length $\langle \ell \rangle$, as a function of the pressure, for different metals at 313 K. CO_2 molecules undergo polymerization beyond a threshold pressure, leading to a sharp (but finite) increase of the mean chain length. This sharp increase results in the steplike feature of the isotherm (Langmuir-type behavior is recovered when $K_1 \gtrsim K_{int}$). The rise is gradual when chain end points are energetically equivalent to internal points (see Supplemental Material [33], Fig. S5). In the infinite-pressure limit, the mean chain length tends to a finite value $\langle \ell \rangle_\infty$ [given by Eq. (S15) in Supplemental Material [33]]. For Mg and Mn at 313 K, for instance, $\langle \ell \rangle_\infty \approx 53$ and 22 μm, respectively (the typical grain size in experiments is ~ 10 μm [17]).

In Fig. 3(c), we show that the bond-bond correlation length (the distance over which fluctuations of bond occupancies are correlated) displays a (nondiverging) maximum at the step position (see Supplemental Material [33], Sec. S8). The behavior shown in Fig. 3 looks superficially like a phase transition, but it is not: Both the mean length of chains and the bond-bond correlation length remain finite. Figure S9 [33] shows that the size-scaling properties of polymerization are distinct from those

of a phase transition; these predicted trends could be assessed experimentally given sufficient control over the MOF grain size.

Conclusions.—We have used a combination of quantum and statistical mechanics to show that cooperative CO_2 adsorption in the class of diamine-appended metal-organic frameworks does not require an underlying phase transition—it results from an abrupt (but finite) change, with pressure, of the mean length of ammonium carbamate chains resident within the framework. Our calculations provide a microscopic understanding of each feature of the isotherm and so suggest how to alter these features for experimental convenience. For instance, the adsorption isotherm can be made more abrupt by increasing the penalty for chain end points—see Fig. S5 [33]. In addition, an understanding of cooperativity in these systems suggests ways of inducing cooperativity in gas-framework combinations in which it is absent [e.g., mmen-Ni_2(dobpdc)], e.g., by introducing binding agents that encourage chain polymerization (see Supplemental Material [33], Sec. S6 and Fig. S6). A similar mechanism may explain why CO_2 uptake in mmen-Ni_2(dobpdc) is enhanced in the presence of H_2O [31]. Our model can be used to predict isotherms for other frameworks within the same class, e.g., with different ligands or metals. Future work will focus on investigating the kinetics of polymerization in these frameworks.

---

*jkundu@lbl.gov
†dgprendergast@lbl.gov
‡swhitelam@lbl.gov

[1] D. Britt, H. Furukawa, B. Wang, T. G. Glover, and O. M. Yaghi, Proc. Natl. Acad. Sci. U.S.A. **106,** 20637 (2009).

[2] W. L. Queen, M. R. Hudson, E. D. Bloch, J. A. Mason, M. I. Gonzalez, J. S. Lee, D. Gygi, J. D. Howe, K. Lee, T. A. Darwish, M. James, V. K. Peterson, S. J. Teat, B. Smit, J. B. Neaton, J. R. Long, and C. M. Brown, Chem. Sci. **5,** 4569 (2014).

[3] K. Sumida, D. L. Rogow, J. A. Mason, T. M. McDonald, E. D. Bloch, Z. R. Herm, T.-H. Bae, and J. R. Long, Chem. Rev. **112,** 724 (2012).

[4] H. Furukawa, K. E. Cordova, M. O'Keeffe, and O. M. Yaghi, Science **341,** 1230444 (2013).

[5] H. Li, M. Eddaoudi, M. O'Keeffe, and O. M. Yaghi, Nature (London) **402,** 276 (1999).

[6] N. L. Rosi, J. Eckert, M. Eddaoudi, D. T. Vodak, J. Kim, M. O'Keeffe, and O. M. Yaghi, Science **300,** 1127 (2003).

[7] MOFs can also be productively used out of equilibrium: see, e.g., Refs. [8,9].

[8] P. Canepa, N. Nijem, Y. J. Chabal, and T. Thonhauser, Phys. Rev. Lett. **110,** 026102 (2013).

[9] J. Kundu, T. Pascal, D. Prendergast, and S. Whitelam, Phys. Chem. Chem. Phys. **18,** 21760 (2016).

[10] S. R. Caskey, A. G. Wong-Foy, and A. J. Matzger, J. Am. Chem. Soc. **130,** 10870 (2008).

[11] S. Xiang, S. He, Z. Zhang, H. Wu, W. Zhou, R. Krishna, and B. Chen, Nat. Commun. **3,** 954 (2012).

[12] P. Nugent, Y. Belmabkhout, S. D. Burd, A. J. Cairns, R. Luebke, K. Forrest, T. Pham, S. Ma, B. Space, L. Wojtas, M. Eddaoudi, and M. J. Zaworotko, Nature (London) **495,** 80 (2013).

[13] H. Furukawa and O. M. Yaghi, J. Am. Chem. Soc. **131,** 8875 (2009).

[14] H. Deng, C. J. Doonan, H. Furukawa, R. B. Ferreira, J. Towne, C. B. Knobler, B. Wang, and O. M. Yaghi, Science **327,** 846 (2010).

[15] D. A. Reed, B. K. Keitz, J. Oktawiec, J. A. Mason, T. Runčevski, D. J. Xiao, L. E. Darago, V. Crocellà, S. Bordiga, and J. R. Long, Nature (London) **550,** 96 (2017).

[16] J. A. Mason, J. Oktawiec, M. K. Taylor, M. R. Hudson, J. Rodriguez, J. E. Bachman, M. I. Gonzalez, A. Cervellino, A. Guagliardi, C. M. Brown, P. L. Llewellyn, N. Masciocchi, and J. R. Long, Nature (London) **527,** 357 (2015).

[17] T. M. McDonald, J. A. Mason, X. Kong, E. D. Bloch, D. Gygi, A. Dani, V. Crocellà, F. Giordanino, S. O. Odoh, W. S. Drisdell, B. Vlaisavljevich, A. L. Dzubak, R. Poloni, S. K. Schnell, N. Planas, K. Lee, T. Pascal, L. F. Wan, D. Prendergast, J. B. Neaton *et al.,* Nature (London) **519,** 303 (2015).

[18] H. Jo, W. R. Lee, N. W. Kim, H. Jung, K. S. Lim, J. E. Kim, D. W. Kang, H. Lee, V. Hiremath, J. G. Seo, H. Jin, D. Moon, S. S. Han, and C. S. Hong, ChemSusChem **10,** 541 (2017).

[19] B. C. Serre, S. Bourrelly, A. Vimont, N. A. Ramsahye, G. Maurin, P. L. Llewellyn, M. Daturi, Y. Filinchuk, O. Leynaud, P. Barnes, and G. Férey, Adv. Mater. **19,** 2246 (2007).

[20] M. Alhamami, H. Doan, and C.-H. Cheng, Materials **7,** 3198 (2014).

[21] W. Yang, A. J. Davies, X. Lin, M. Suyetin, R. Matsuda, A. J. Blake, C. Wilson, W. Lewis, J. E. Parker, C. C. Tang, M. W. George, P. Hubberstey, S. Kitagawa, H. Sakamoto, E. Bichoutskaia, N. R. Champness, S. Yang, and M. Schroder, Chem. Sci. **3,** 2993 (2012).

[22] C. M. Simon, E. Braun, C. Carraro, and B. Smit, Proc. Natl. Acad. Sci. U.S.A. **114,** E287 (2017).

[23] F.-X. Coudert, M. Jeffroy, A. H. Fuchs, A. Boutin, and C. Mellot-Draznieks, J. Am. Chem. Soc. **130,** 14294 (2008).

[24] C. Triguero, F.-X. Coudert, A. Boutin, A. H. Fuchs, and A. V. Neimark, J. Phys. Chem. Lett. **2,** 2033 (2011).

[25] D. Bousquet, F.-X. Coudert, A. G. J. Fossati, A. V. Neimark, A. H. Fuchs, and A. Boutin, J. Chem. Phys. **138,** 174706 (2013).

[26] A. Ghysels, L. Vanduyfhuys, M. Vandichel, M. Waroquier, V. V. Speybroeck, and B. Smit, J. Phys. Chem. C **117,** 11540 (2013).

[27] L. J. Dunnea and G. Manos, Dalton Trans. **45,** 4213 (2016).

[28] J. Seo, R. Matsuda, H. Sakamoto, C. Bonneau, and S. Kitagawa, J. Am. Chem. Soc. **131,** 12792 (2009).

[29] B. Vlaisavljevich, S. O. Odoh, S. K. Schnell, A. L. Dzubak, K. Lee, N. Planas, J. B. Neaton, L. Gagliardi, and B. Smit, Chem. Sci. **6,** 5177 (2015).

[30] N. Goldenfeld, *Lectures on Phase Transitions and the Renormalization Group* (Addison-Wesley, Reading, MA, 1992).

[31] J. A. Mason, T. M. McDonald, T.-H. Bae, J. E. Bachman, K. Sumida, J. J. Dutton, S. S. Kaye, and J. R. Long, J. Am. Chem. Soc. **137,** 4787 (2015).

[32] J. D. Martell, L. B. Porter-Zasada, A. C. Forse, R. L. Siegelman, M. I. Gonzalez, J. Oktawiec, T. Runcevski, J. Xu, M. Srebro-Hooper, P. J. Milner, K. A. Colwell, J. Autschbach, J. A. Reimer, and J. R. Long, J. Am. Chem. Soc. **139,** 16000 (2017).

[33] See Supplemental Material at http://link.aps.org/supplemental/10.1103/PhysRevLett.121.015701 for detailed discussions on DFT calculation, transfer matrix formalism, fine details of isotherms, calculation of chain-length distribution, correlation length and finite size effects.

[34] P. M. Pfeuty and J. C. Wheeler, Phys. Rev. A **27,** 2178 (1983).

[35] $q_{\text{inter}} = q_{\text{rot}}q_{\text{vib}} = [(8\pi^2 I k_B T)/(\sigma h^2)] \prod_{j=1}^{4}\{[\exp(-\theta_{\text{vib},j}/2T)]/[1 - \exp(-\theta_{\text{vib},j}/2T)]\}$, where q_{rot} and q_{vib} are the rotational and vibrational partition functions, respectively, of a CO_2 molecule, I is the moment of inertia, and $\sigma(=2)$ is the symmetry factor of CO_2. ($\theta_{\text{vib},j} = h\nu_j/k_B$; ν_j corresponds to the frequency of the jth normal mode of vibration).

[36] This approximation is reasonable, because cooperative behavior in the experiment is observed at pressures of 1 bar or below, where CO_2 behaves as an ideal gas; using the Peng-Robinson equation of state for CO_2 we checked that the fugacity coefficient of CO_2 at 1 bar is ≈ 0.99.

[37] $K_\alpha = g_\alpha W_\alpha = V_\alpha \Lambda^{-3} q_{\text{inter},\alpha} \exp(\beta\mu) \exp(-\beta E_\alpha) = V_\alpha \Lambda^{-3} q_{\text{inter},\alpha} (\beta P \Lambda^3 q_{\text{inter,bulk}}^{-1}) e^{-\beta E_\alpha} \approx \beta P V_\alpha e^{-\beta E_\alpha}$.

[38] J. F. Stilck, M. A. Neto, and W. G. Dantas, Physica A (Amsterdam) **368**, 442 (2006).